

FEEDBACK PROCESSES IN EARLY-TYPE GALAXIES

IGNACIO FERRERAS,¹ EVAN SCANNAPIECO,^{2,3} AND JOSEPH SILK¹

Received 2002 April 9; accepted 2002 July 12

ABSTRACT

We present a simple phenomenological model of feedback in early-type galaxies that tracks the evolution of the interstellar medium gas mass, metallicity, and temperature. Modeling the star formation rate as a Schmidt law with a temperature-dependent efficiency, we find that intermittent episodes of star formation are common in moderate-size ellipticals. Our model is applicable in the case in which the thermalization time from supernovae is sufficiently long that spatial variations are relatively unimportant, an appropriate assumption for the empirical parameters adopted here, but one that can only be demonstrated conclusively through more detailed numerical studies. The departure from a standard scenario of passive evolution implies significantly younger luminosity-weighted ages for the stellar populations of low-mass galaxies at moderate redshifts, even though the more physically meaningful mass-weighted ages are changed only slightly. Secondary bursts of star formation also lead to a natural explanation of the large scatter in the near-UV–optical relation observed in clusters at moderate redshift and account for the population of E+A galaxies that display a spheroidal morphology. As the late-time formation of stars in our model is due to the gradual cooling of the interstellar medium, which is heated to temperatures ~ 1 keV by the initial burst of supernovae, our conclusions do not rely on any environmental effects or external mechanisms. Furthermore, a simple estimate of the X-ray emission from this supernova-heated gas leads to an L_X - L_B correlation that is in good agreement with observed values. Thus, feedback processes may be essential to understanding the observed properties of early-type galaxies from the optical to the X-ray.

Subject headings: galaxies: elliptical and lenticular, cD — galaxies: evolution — galaxies: stellar content

1. INTRODUCTION

Of all the fields of astronomy, the study of galaxy formation may be the one in which the rift between theory and observation is the most difficult to bridge. Theoretical astrophysicists, perhaps from a temperamental as well as a practical point of view, are best at predicting the most difficult component of the universe to measure: the overall distribution of invisible “dark matter.” While the evolution of this component is well understood, numerical and analytical models must stretch their predictive powers to the limit to superimpose on this history the messy heating, cooling, and enrichment processes that affect baryonic gas.

At the same time, observational astrophysicists, perhaps from a romantic as well as a practical point of view, are happiest when looking at the most complicated thing they could ever measure: the stars in the night sky. A proverbial tail that wags the dog, the magnitudes and colors of the stellar populations in galaxies are dependent on not only the history of the baryonic gas but also the notoriously complicated process of star formation. As many possible environmental effects can have an unknown impact on the number and distribution of stars formed (see, e.g., Kroupa 2001; Larson 1999; Scalo 1998), which is even more uncertain under primordial conditions (see, e.g., Nakamura & Umemura 2001), predicting the optical properties of galaxies involved from “first principles” requires an enormous amount of extrapolation and simplifying assumptions.

This great rift calls for astronomers to work to meet each other from each side of the divide. Thus, simulations and semianalytical models of galaxy formation are continuously striving to include all the important physical processes that affect forming galaxies and the surrounding intergalactic medium (e.g., Kauffmann et al. 1999; Baugh et al. 1998; Somerville & Primack 1999). From the observational point of view, astronomers must constantly develop more careful phenomenological models, which better express the features seen in simulations: making statements as to the ages of stars, their metallicities, and levels of dust extinction, rather than simply considering their infrared, optical, and ultraviolet colors and magnitudes. Models of this sort include Tinsley (1980), Matteucci & Tornambé (1987), Tantaló et al. (1998), and Ferreras & Silk (2000c).

From a theoretical point of view, one of the most important issues to recently come to the fore is the role of supernova (SN) feedback in galaxy formation. N -body simulations have shown that the baryonic components of galaxies that form in cold dark matter (CDM) simulations systematically lose too much of their angular momentum to the dark matter halos in which they are contained (Navarro & Benz 1991). As discussed in White (1994), the resolution of this problem is widely believed to be the inclusion of feedback, although the proper modeling of this process remains a subject of intense debate. Thus, since the first numerical model of thermal heating by Katz (1992), approaches have included implementation of kinetic boosts (Mihos & Hernquist 1994; Gerritsen 1997), a multiphase model of star formation and feedback (Yepes et al. 1997; Hultman & Pharasyn 1999), a model of turbulent pressure support from feedback (Springel 2000), and a model in which energy persists in the interstellar medium (ISM) for a period corresponding to the lifetime of stellar associations (Thacker & Couchman 2001). Finally, feedback processes are likely to

¹ Nuclear and Astrophysics Laboratory, Keble Road, Oxford OX1 3RH, England, UK; ferreras@astro.ox.ac.uk, silk@astro.ox.ac.uk.

² Department of Astronomy, 601 Campbell Hall 3411, University of California, Berkeley, CA 94720; evan@arcetri.astro.it.

³ Osservatorio Astrofisico di Arcetri, 50125 Florence, Italy.

play a more general role in impacting the intergalactic medium and conditions under which galaxy formation occurs (Mac Low & Ferrara 1999; Martel & Shapiro 2001; Scannapieco & Broadhurst 2001; Scannapieco, Thacker, & Davis 2001).

Yet despite the many exploratory feedback models being examined theoretically, the role of feedback in empirical modeling has been more limited. Ferreras & Silk (2000b, 2001) explored a simple model in which feedback was included phenomenologically using two free parameters: the star formation efficiency and the fraction of gas ejected in outflows. These values are dependent on the thermal and mechanical feedback from SNe, but they fail to capture the impact of the state of the ISM itself, despite the close relationship between this state and star formation (McKee & Ostriker 1977). Our primarily theoretical motivation in this paper, then, is to extend these models by tracking the temperature evolution of the ISM, taking into account the thermal contributions of SNe and metallicity-dependent gas cooling.

The primarily observational motivation for this paper, on the other hand, is the measurement of a large scatter at the faint end of the near-ultraviolet (NUV) minus optical color-magnitude relation in cluster A851 ($z = 0.4$) observed by Ferreras & Silk (2000b) using passbands F300W and F702W of the WFPC2 on board the *Hubble Space Telescope*. A simple analysis of this scatter shows that it cannot be accounted for by old horizontal branch stars. Moreover, significantly younger luminosity-weighted ages were found, although a degeneracy between the age of the young stellar component and its mass fraction prevented a detailed estimate of a more physically meaningful mass-weighted age. This result shows that the star formation history of early-type galaxies is much more complicated than the standard picture in which a single stellar population formed at a redshift $z \gtrsim 3$ and then evolved passively.

The structure of this work is as follows. In § 2 we describe a simple thermal model of SN feedback in elliptical galaxies and its impact on the gas, stellar, and metallicity evolution of these objects. In § 3 we describe the general features of our model and the physics on which they depend. Our evolutionary tracks are combined with population synthesis models in § 4 and used to study the color-magnitude relationship in ellipticals in both the optical and NUV. In § 5 we examine the compatibility of our model with X-ray observations of early-type galaxies. In § 6 we discuss the implications of our modeling for future observational studies of feedback in ellipticals as well as how our model compares to other theoretical approaches, and conclusions are given in § 7.

2. THERMAL MODEL OF FEEDBACK IN ELLIPTICAL GALAXIES

2.1. Basic Assumptions

In order to reconstruct the star formation and chemical enrichment of early-type galaxies, we follow an approach similar to that adopted in Ferreras & Silk (2000c), which in turn is an adaptation of the formalism of Tinsley (1980) in which the evolution within a galaxy is reduced to a few general parameters. Our model consists of only gas and stars. For each component we trace the net metallicity, counting all elements heavier than helium in the same way. The mass

in gas, $M_g(t)$, and in stars, $M_s(t)$, in each model is normalized to the initial total gas mass M_{g0} such that $\mu_g(t) \equiv M_g(t)/M_{g0}$ and $\mu_s(t) \equiv M_s(t)/M_{g0}$.

The gas component is fueled by infall of pre-enriched gas at a rate assumed to be a Gaussian function:

$$f(t) \propto \frac{1}{\tau_f \sqrt{2\pi}} \exp \left[-\frac{(t - t_{f0})^2}{2\tau_f^2} \right], \quad (1)$$

where τ_f is the infall timescale and t_{f0} is the epoch of maximum infall, parameterized in terms of a formation redshift z_F such that $t(z_F) = t_{f0}$. We additionally assume a Salpeter (1955) initial mass function (IMF) with cutoffs at 0.1 and 100 M_\odot and an initial metallicity of the infall gas of $Z_0 = Z_\odot/10$. This value is motivated by Renzini (1999), who used an estimated $Z_\odot/3$ metallicity of the $z = 0$ universe and the fact that $\sim 30\%$ of all stars have formed at $z \gtrsim 3$ to imply that the average metallicity of the high-redshift universe is $\sim \frac{1}{3} \times \frac{1}{3} \sim 1/10 Z_\odot$. Similar levels of pre-enrichment are consistent with the observed lack of G dwarf stars with metallicities below $\sim 0.1 Z_\odot$ in the Milky Way disk and the paucity of such stars in other massive early- and late-type galaxies (Worthey, Dorman, & Jones 1996; Thomas, Greggio, & Bender 1999).

2.2. Gas and Stellar Evolution

We consider an infall model in which the star formation efficiency is determined by the temperatures of the gas. In this case the limiting factor in star formation is not the conversion of cool gas into stars, but rather the cooling of the gas itself into molecular clouds. We write the star formation rate as a Schmidt law with respect to the normalized gas mass:

$$\psi(t) = C_{\text{eff}}(T) \mu_g^{\mathcal{N}}(t), \quad (2)$$

where $C_{\text{eff}}(T)$ is the temperature-dependent star formation efficiency and $1 < \mathcal{N} < 2$. A comparison of the Schmidt law with the observed star formation rate in local galaxies gives a value $\mathcal{N} \sim 1.5$ (Kennicutt 1998), adopted throughout this paper. We assume a Fermi step function for the dependence of the star formation efficiency on the temperature:

$$C_{\text{eff}}(T_4) = \frac{C_{\text{eff}}^0}{1 + \exp[(T_4 - 1)/\alpha]}, \quad (3)$$

where $T_4 \equiv T/10^4$ K and α is a parameter that controls the steepness of the step. This function assumes that the star formation efficiency decreases abruptly for an average temperature of the ISM above $T_4 \sim 1$, chosen to correspond to the temperature at which hydrogen is ionized. Finally, we assume fixed values for the normalization ($C_{\text{eff}}^0 = 100$) and the steepness of the step ($\alpha = 3$).

With these definitions the equations for the evolution of gas and stars can be written as a sum of gas accretion, star formation, and ejection of material from stars:

$$\frac{d\mu_g}{dt} = f(t) - C_{\text{eff}}(T_4) \mu_g^{\mathcal{N}} + (1 - B_{\text{out}}) E(t), \quad (4)$$

$$\frac{d\mu_s}{dt} = C_{\text{eff}}(T_4) \mu_g^{\mathcal{N}} - E(t), \quad (5)$$

where the integral $E(t)$ is the mass of gas ejected at a time t

from stars at the end of their lifetimes:

$$E(t) = \int_{m_i}^{\infty} dm \phi(m) (m - w_m) \psi(t - \tau_m - \tau_{\text{SN}}), \quad (6)$$

where $\phi(m)$ is the IMF, w_m is the mass of a stellar remnant with an initial mass m , and m_i is the mass corresponding to a stellar lifetime t , each of which can be fixed using the values as in Ferreras & Silk (2000c). A delay τ_{SN} is included to account for the fact that it takes some time for the energy from SNe to spread throughout the galaxy. This should be roughly equal to the time it takes for a gas bubble heated by the surrounding SN ejecta to percolate throughout the ISM of the galaxy, which we estimate to be $\tau_{\text{SN}} \sim 100$ Myr. Finally, B_{out} is the fraction of gas ejected in outflows, as discussed in Ferreras & Silk (2000c). This parameter is a decreasing function of galaxy mass that lies in the range $0 \leq B_{\text{out}} \leq 1$ and determines the average metallicity of the stellar populations. This inefficiency of metal ejection in large ellipticals is thought to be the best explanation of the correlation between mass and metallicity (Arimoto & Yoshii 1987), which gives rise to the color-magnitude relation.

2.3. Thermal Feedback

In order to model the temperature evolution of the gas, we consider the cooling and heating sources that contribute to its total energy content. Defining \mathcal{E} as the total internal energy, we find

$$\frac{d\mathcal{E}}{dt} = -N_e n_e \Lambda(T, Z) + \frac{f}{M_{\odot}} k T_f + \epsilon 10^{51} \text{ ergs } \frac{M_{g0}}{M_{\odot}} R_{\text{SN}}, \quad (7)$$

where N_e and n_e are the total number and number density of electrons, respectively, T_f is the temperature of the infalling gas, and ϵ is the fraction of the SN energy that goes toward heating the gas. The three terms on the right-hand side of this equation correspond to radiative cooling in the gas, thermal input from infalling gas, and energy input from SNe, respectively.

The first of these is proportional to the electron density of the gas squared times the radiative cooling function, which is dependent on both the temperature and overall metallicity of the gas. In our simple model, we assume a polytropic equation so that $n_e \propto T^{1/(\gamma-1)}$. The value of the polytropic index γ depends on the state of the ISM as shown below. The cooling function, on the other hand, can be calculated directly according to the tabulated model in Sutherland & Dopita (1993), which assumes solar abundance ratios.

In the second term, we take T_f to be the virial temperature of the halo; in the last term, R_{SN} is the rate of SNe in the galaxy and ϵ is the fraction of the resulting mechanical energy that is deposited into the gas. In calculating R_{SN} we consider contributions from both Type II and Type Ia SNe, such that $R_{\text{SN}}(t) = R_{\text{II}}(t) + R_{\text{Ia}}(t)$. The first of these contributions can be written as

$$R_{\text{II}}(t) = \int_{8 M_{\odot}}^{100 M_{\odot}} dm \phi(m) C_{\text{eff}} [T_4(t - \tau_m \tau_{\text{SN}})] \mu_g^{\nu} \times (t - \tau_m - \tau_{\text{SN}}), \quad (8)$$

where the integral gives the contribution from massive stars that undergo core collapse.

In the Type Ia case, we follow the standard prescription of Greggio & Renzini (1983), recently explored in more detail by Matteucci & Recchi (2001). In this model the rate is written with respect to the distribution function of binary systems that can harbor a white dwarf:

$$R_{\text{Ia}}(t) = \mathcal{A} \int_{m_i}^{16 M_{\odot}} dm \phi(m) \int_{\mu(m)}^{\mu_{\text{max}}} d\mu' f(\mu') \psi \times (t - \tau_m - \tau_{\text{SN}}), \quad (9)$$

where $m_i = \max[3 M_{\odot}, m(t)]$ and μ is the ratio of the mass of the secondary star and the total, which ranges in the integral from $\mu(m) = \max(1 - 8/m, 0.8/m)$ to $\mu_{\text{max}} = 0.5$. Finally, $f(\mu) = 2^{1+\beta}(1 + \beta)\mu^{\beta}$ is the distribution function of binaries that is taken from Greggio & Renzini (1983), with $\beta = 2$. The normalization in this case is taken to be $\mathcal{A} = 0.05$, calibrated from the ratio of Type Ia to Type II SNe that best fits solar abundances $N(\text{Ia})/N(\text{II}) = 0.12$ (Nomoto, Iwamoto, & Kishimoto 1997).

In order to compute the evolution of the temperature, we assume an ideal gas ($p = nkT$), with an equation of state given by $p \propto n^{\gamma}$, which implies $T \propto n^{\gamma-1}$. Writing

$$d\mathcal{E} = \frac{3}{2} Nk dT - p dV, \quad (10)$$

we find

$$\frac{d\mathcal{E}}{kN} = dT \left(\frac{3}{2} + \frac{1}{\gamma-1} \right). \quad (11)$$

During the formation history of the galaxy we assume a single equation of state, namely, that of an ideal gas at constant pressure. Hence, we fix $\gamma = 0$ throughout. This is motivated by cooling timescales that are much longer than the dynamical time. Rewriting the feedback efficiency in terms of the fraction of gas ejected in outflows and solving for the temperature in terms of T_4 , the evolution of the gas temperature becomes

$$2\mu_g \frac{dT_4}{dt} = (1 - B_{\text{out}}) m_{0.7} T_{\text{SN}} (R_{\text{II}} + R_{\text{Ia}}) - [\psi - (1 - B_{\text{out}})E] T_4 - \frac{T_4}{\tau_{\text{cool}}} \frac{N_e \mu_g}{N_g} + f(T_f - T_4), \quad (12)$$

where $m_{0.7}$ is the mean mass of a gas particle in units of 0.7 times the proton mass (note that this gas is ionized), $\tau_{\text{cool}} \equiv kT/n\Lambda$ is the cooling timescale, and $T_{\text{SN}} \sim 3 \times 10^5$ (in units of 10^4 K) is again the energy input from SNe, now rescaled in terms of an SN ‘‘temperature,’’ which corresponds to a thermal efficiency of $\epsilon = 0.7(1 - B_{\text{out}})$.

Note that our model ignores the thermal contribution from the ejecta of intermediate- and low-mass stars. This approximation is based on the assumption that the temperatures of planetary nebulae are much less than the typical temperature of gas in the galaxy.

2.4. Chemical Enrichment

The final element of our model is the evolution of metals in the gas. In this case the relevant equation is

$$\frac{d(Z_g \mu_g)}{dt} = Z_f f - Z_g C_{\text{eff}}(T) \mu_g^{\nu} + (1 - 1.2 B_{\text{out}}) (E_Z + y_{\text{Ia}} R_{\text{Ia}}), \quad (13)$$

where $Z_f = 0.1 Z_\odot$ is the metallicity of the pre-enriched infalling gas. Note that each of these terms parallels those in equation (4). In equation (13) E_Z is the amount of metals ejected from stars:

$$E_Z(t) \equiv \int_{m_i}^{\infty} dm \phi(m) \psi(t - \tau_m - \tau_{\text{SN}}) \times [(m - w_m - mp_m) Z_g(t - \tau_m - \tau_{\text{SN}}) + mp_m], \quad (14)$$

where the fraction of a star of mass m transformed into metals is given by p_m . For intermediate-mass stars, with $M \leq 8 M_\odot$ we use a power-law fit to the yields from Renzini & Voli (1981), Marigo, Bressan, & Chiosi (1996), and van den Hoek & Groenewegen (1997). For larger stars, which contribute to metal enrichment via Type II SNe, the yields are taken from Woosley & Weaver (1995) and Thielemann, Nomoto, & Hashimoto (1996). Note that the differences in the yields between these two groups are due to the different physical inputs assumed, mainly the criterion for convection, the nuclear reaction rates, and the determination of the upper mass cut. Finally, the $(1 - 1.2B_{\text{out}})$ factor in equation (13) accounts for the fact that outflows driven by SN-induced winds are likely to be enriched with metals, as described by Vader (1986).

Finally, Type Ia SNe must be added to the chemical enrichment process. Using the rate of SNe, $R_{\text{Ia}}(t)$, as given by equation (9), we include the contribution to the metallicity of the gas, assuming that the yield from each Type Ia SN is $y_{\text{Ia}} = 0.6 M_\odot$ (mostly iron; Thielemann, Nomoto, & Yokoi 1986). There is no such term in the equation tracing the evolution of gas, equation (4), however, since this type of SN does not contribute to the gas reservoir. The standard progenitor of a Type Ia SN is a binary system with a C-O white dwarf. Given that the maximum initial stellar mass that leads to a white dwarf is approximately $8 M_\odot$, this means that Type Ia SNe begin to contribute 0.03 Gyr after stars are first formed.

2.5. The Formation Epoch of Ellipticals

In keeping with our desire to incorporate both observational and theoretical advances into our simple model, we do not apply the usual observational benchmark of a fixed formation epoch but instead allow for a range of formation redshifts corresponding to the theoretically favored model of hierarchical structure formation. In this case we allow the formation redshift to be a function of the virial temperature and choose $z_F(T_{\text{vir}})$ such that the probability of forming a galaxy at z_F is the same for all values of T_{vir} . Throughout this paper, the formation redshift corresponds to the epoch of maximum gas infall.

We restrict our attention to the currently favored Λ CDM model of structure formation, which is described in detail in Eisenstein & Hu (1999). In this model, objects that are equally likely to form have the same value of $\sigma(R)D(z_F)$, where $\sigma(R)$ is the amplitude of mass fluctuations inside a sphere of radius R extrapolated linearly to $z = 0$, given by their equations (34) and (35), and D is a “growth factor” that tracks the linear growth of perturbations as a function of redshift, given by their equation (10). Based mainly on the most recent measurements of the cosmic microwave background (Balbi et al. 2000; Netterfield et al. 2002; Pryke et al. 2002), we consider a cosmological model in which

$\Omega_m = 0.35$, $\Omega_\Lambda = 0.65$, $\Omega_b = 0.06$, $\sigma_8 = 0.87$, $\Gamma = 0.18$, $n = 1$, and $h = 0.65$, where Ω_m , Ω_Λ , and Ω_b are the total matter, vacuum, and baryonic densities in units of the critical density, respectively, σ_8 is $\sigma(r)$ at the $8 h^{-1}$ Mpc scale, h is the Hubble constant in units of $100 \text{ km s}^{-1} \text{ Mpc}^{-1}$, and n is the “tilt” of the primordial power spectrum, where $n = 1$ corresponds to a scale-invariant spectrum. The age of the universe in this cosmology is ~ 14 Gyr.

Using this model, we select a range of objects and determine z_F and T_4 parametrically as a function of total mass, which is not itself observable. To calculate z_F , we compute the radius of the perturbation, R , as $0.95 \Omega_m^{-1/3} M_{12}^{1/3} h^{-1}$ Mpc, where M_{12} is the mass in units of $10^{12} h^{-1} M_\odot$, and then invert $\sigma(R)D(z_F) = \text{const}$. Similarly, we calculate T_4 from a standard model of collapse and virialization, which has been shown to be in good agreement with more detailed numerical simulations (see, e.g., Eke, Cole, & Frenk 1996). In this case

$$T_4 = (90 \text{ K}) M_{12}^{2/3} (1 + z_F) [\Omega_m + \Omega_\Lambda (1 + z_F)^{-3}]^{1/3}. \quad (15)$$

Finally, we select $\sigma(R)D(z_F)$ such that the largest objects we consider—for which $T_4 = 300$ —form at a redshift of $z_F = 2$, leading to a range of formation redshifts from 2 to 4.4 (at $T_4 = 30$). Note that in this case ellipticals are formed from the so-called rare peaks at redshifts at which the mean amplitude of mass fluctuations, $\sigma(R)D(z_F)$, is 2.5 times smaller than the critical value for collapse and virialization. This is consistent with hierarchical models that predict ellipticals to form at the peaks of the density distribution as a result of their clustering properties and the fact that such perturbations are likely to undergo a “major merger” (see, e.g., Kauffmann & Charlot 1998).

3. INTERMITTENT STAR FORMATION IN ELLIPTICAL GALAXIES

3.1. Global Parameters and Features of Feedback Models

In this section we describe the main features of our model and the physics on which they depend. In Table 1 we list the model parameters that are independent of mass. The first two of these, $\mathcal{N} = 1.5$ and $Z_0 = Z_\odot/10$, are set to canonical values consistent with a variety of observations. The SN parameters $T_{\text{SN},4}$ and τ_{SN} , on the other hand, are based on simple estimates of the thermal energy released by each SNe and the time delay for this energy to be transferred to the ISM of the galaxy. Finally, the thermal SF efficiency C_{eff}^0 and steepness α are arbitrary parameters in our model, whose values we have fixed after an extensive search of parameter space.

TABLE 1
MASS-INDEPENDENT MODEL PARAMETERS

Parameter	Value
Schmidt law index (\mathcal{N}).....	1.5
Pre-enrichment (Z_0).....	$Z_\odot/10$
SN temperature ($T_{\text{SN},4}$).....	3×10^5
SN delay (τ_{SN}) (Myr).....	100
SF efficiency (C_{eff}^0).....	100
Efficiency steepness (α).....	3

Having established these values, we show in Figure 1 the model prediction for the evolution of a massive elliptical galaxy ($n_0 = 2$, $B_{\text{out}} = 0$, $T_0 = 300$, $z_F = 2$). This object undergoes a number of bursts of star formation at roughly constant time intervals from its formation redshift of $z_F = 2$ until the temperature of the ISM rises above ~ 1 keV. Notice that the feedback cycles generated by our model are quite punctuated, with the gas remaining at high temperatures for the majority of their evolution, interrupted by brief intervals of “catastrophic” cooling that result in new bursts of star formation. Each burst is followed by a new generation of SNe, which quickly heats the ISM back up to the high-temperature state, where it remains quiescent until the next epoch of cooling.

Each phase of this feedback cycle is dependent on the physical parameters of our models. In most cases, this dependence is quite straightforward and can be understood by simple scaling arguments, despite the fact that a more complicated numerical approach is required to study the evolution in detail. Before turning our attention to the observable consequences of our modeling, we first review these dependencies, comparing the properties of the large galaxy shown in Figure 1 with an example of a much smaller object with parameters $n_0 = 0.8$, $B_{\text{out}} = 0.5$, $T_0 = 45$, and $z_F = 3.9$ in Figure 2.

Both of these galaxies start at their virial temperatures and remain there for a significant period of time before undergoing a first burst of star formation. At high tempera-

tures $\gtrsim 10^5$ K, the cooling function Λ roughly scales as $1/T$; thus, the cooling time of the gas $\tau_{\text{cool}} = kT/n\Lambda$ is approximately $\propto T^3$, as $n \propto 1/T$ during the cooling phase. This strong dependence on temperature means that the main barrier to star formation in these objects is the cooling time *at the highest temperature in the feedback cycle*. Once the galaxy cools to temperatures $T \sim 10^4$ K, the sharp decline of the cooling function halts the thermal runaway, while at the same time star formation becomes much more efficient. Note that the strong scaling of the cooling function with temperature means that this lower value is nearly constant over the full range of galaxy masses. It is during this stage that almost all stars are formed, resulting in a starburst with total star formation rates of order $1000 M_\odot \text{ yr}^{-1}$ in massive galaxies and $10 M_\odot \text{ yr}^{-1}$ in low-mass systems. The galaxy remains in a low-temperature state until the first generation of SNe explode and transfer their thermal energy to the gas. Thus, each starburst results in a total fraction of stars created, which is roughly $C_{\text{eff}}(\tau_{\text{SN}} + \tau_{m=100 M_\odot})\mu_g(t_{\text{SB}})$, where $\mu_g(t_{\text{SB}})$ is gas mass at the start of the starburst. Similarly, the poststarburst temperature is simply proportional to the number of stars formed times the energy transferred to the gas: $E \propto (1 - B_{\text{out}})T_{\text{SN}}C_{\text{eff}}(\tau_{\text{SN}} + \tau_{m=100 M_\odot})\mu_g(t_{\text{SB}})$.

From these scalings, it is easy to understand why smaller galaxies oscillate more frequently than those with larger masses. As the energy per SN, star formation efficiency, and τ_{SN} are fixed for all models, the SN energy generated in each model varies only by a factor $(1 - B_{\text{out}})\mu_g(t_{\text{SB}})$. But for each

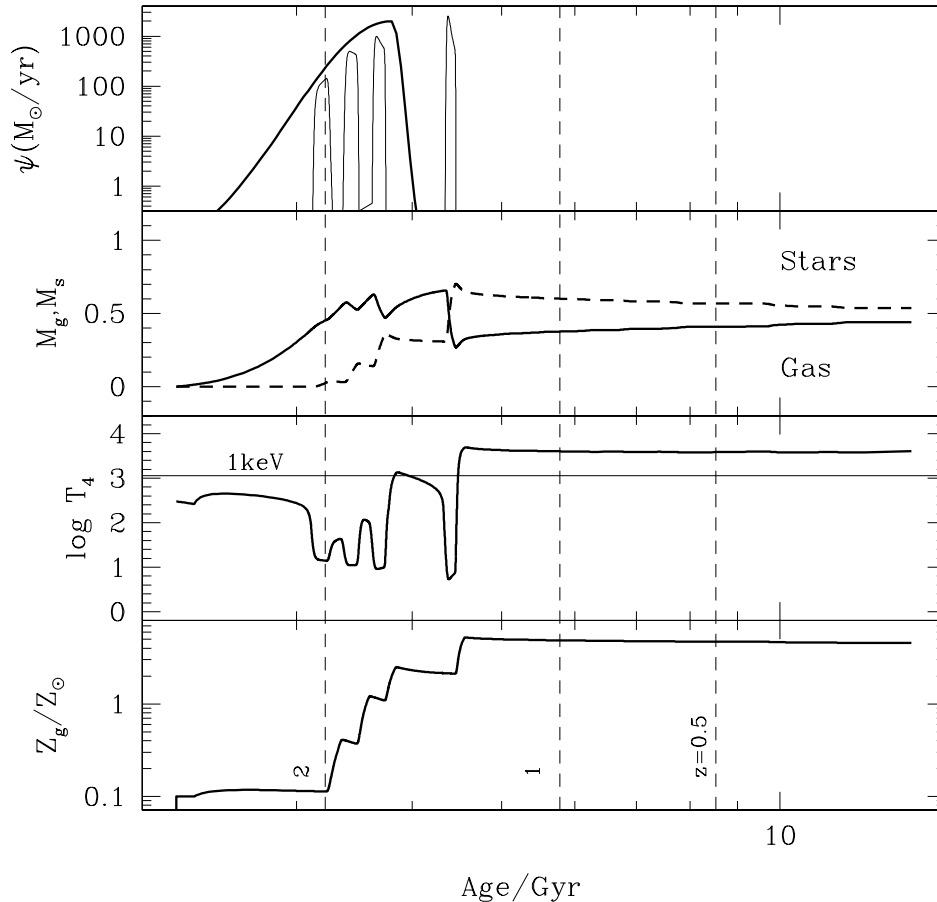


FIG. 1.—Star formation history of a massive elliptical galaxy that corresponds to $T_0 = 300$, $n_0 = 2$, $\tau_f = 0.5$ Gyr, $z_F = 2$, and $B_{\text{out}} = 0$. The photometry at zero redshift, $U-V = 1.55$, $V-K = 3.25$ corresponds to a bright elliptical ($M_V = -22$, $\log \sigma = 2.4$) in a local cluster.

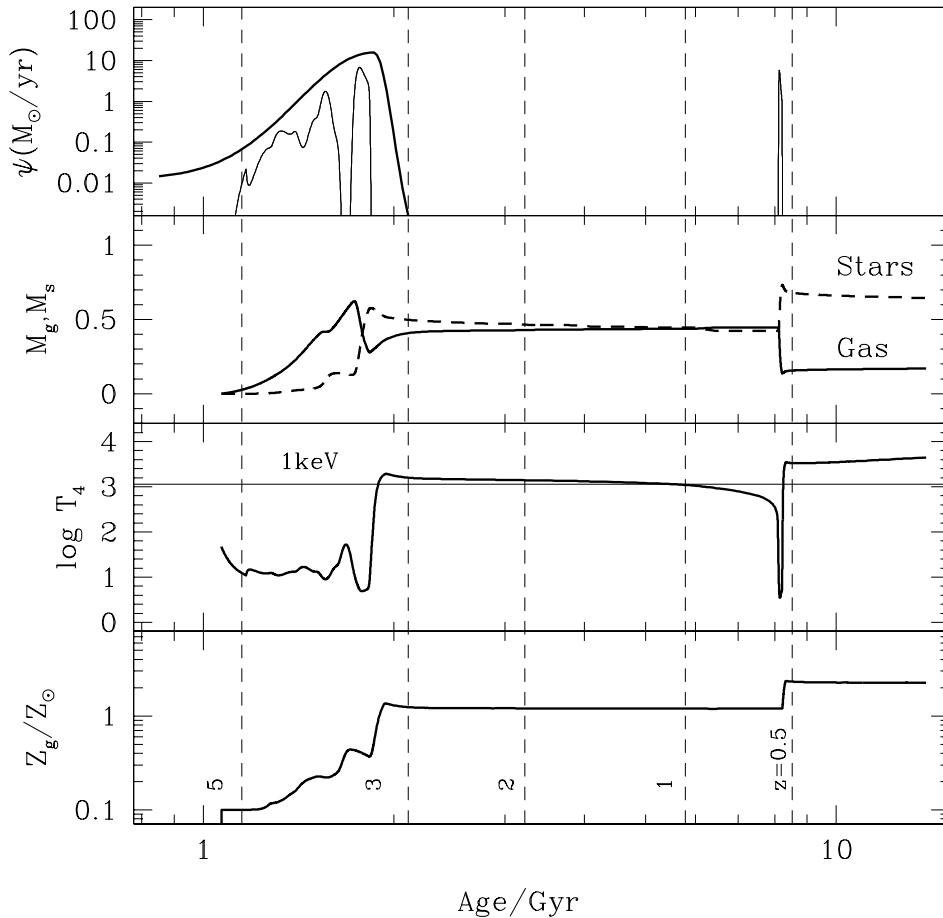


FIG. 2.—Star formation history of a faint elliptical galaxy that corresponds to $T_0 = 45$, $n_0 = 0.8$, $\tau_f = 0.2$ Gyr, $z_F = 3.9$, and $B_{\text{out}} = 0.5$. The photometry at zero redshift, $U-V = 1.2$, $V-K = 2.9$ corresponds to a faint $M_V = -18$ elliptical (i.e., $\log \sigma \sim 1.8$) in a local cluster.

starburst, the ratio of the initial to final gas mass is fixed and the poststarburst temperature scales simply as $\propto (1 - B_{\text{out}})$. Thus, the period between starbursts can be estimated as approximately $\propto T^3 \propto (1 - B_{\text{out}})^3$.

Comparing Figures 1 and 2, which give the star formation histories of two early-type galaxies with very different masses, we see that the ratio of gas outflow fractions is 2, implying that the final bursts of star formation will take place approximately 8 times later in the high-mass galaxy. Thus, the last early burst in the large galaxy takes place after a delay of approximately 1 Gyr, while the last early burst in the $T_4 = 45$ model is partially blended with the peak before it, with a relative separation of approximately $\frac{1}{8}$ Gyr. Similarly, after the early burst stage, the smaller galaxy reaches a temperature of 1.5×10^7 K and cools to form a secondary late burst of star formation after approximately 7 Gyr. On the other hand, the large galaxy reaches a temperature of $\approx 3 \times 10^7$ K after the initial burst phase, corresponding to a cooling time of ~ 50 Gyr, and therefore no late bursts appear in this model.

It is important to note that the relationship between mass and metallicity in our models arises from not only a differential B_{out} , as in Ferreras & Silk (2000c), but also an interplay between the multiple bursts and the infall timescale. This aspect of our model is independent of the late-time star formation properties of these galaxies. Thus, it is conceivable that the early-time star formation history of the galaxy may have been somewhat different (e.g., perhaps as a result of

the merger of two disks) while still preserving the star formation cycles and scalings seen in our models at late times. The metallicity-mass relation is discussed in more detail in § 4.

Finally, in Figures 1 and 2, the thick lines represent an estimate as to the physical star formation rate in these objects. This is likely to be a smoothed version of the theoretical curve, as our model assumes a pointlike galaxy, whereas a more realistic model including spatial information would have bursts of star formation happening at slightly different epochs in different regions of the galaxy. This would result in a more continuous global star formation rate during the first stage, while preserving the punctuated bursts at later times.

This raises the question as to whether the interactions between areas of the galaxy in which star formation is out of phase may be able to suppress the cycles seen in our one-zone models. Here the important issue is whether SNe are able to heat a region of space and suppress star formation fast enough that spatial variations between regions become important. In our one-zone models, we assume a typical delay of 100 Myr for SNe to percolate through the galaxy, dumping a fraction B_{out} of their energy into the ISM. Thus, we expect a one-zone description to be applicable if the galaxy is relatively homogeneous on scales comparable to 100 Myr times the sound speed of the gas. A simple estimate of this speed gives $c_s \approx 10T_4^{1/2}$ km s $^{-1}$; our one-zone approach is equivalent to assuming that the galaxy is relatively

smooth on scales above $\tau_{\text{SN}}c_s \approx 1T_4^{1/2}$ kpc, a reasonably large scale even at $T_4 = 1$. Note however that our value for the SN delay time is somewhat arbitrary and chosen empirically to reproduce the observed properties of elliptical galaxies. Thus, while our model is a plausible description of a more complete treatment, a dedicated numerical study would be necessary to more firmly establish the relevant thermalization time in our models and whether $c_s\tau$ is large enough that spatial variations can be ignored.

3.2. Mass-dependent Parameters and Average Properties

Having examined the main features of our models, we now turn our attention to constructing a representative sample of elliptical galaxies over a range of masses. In Table 2 we list the parameters of our model that depend on age and indicate their scaling with mass and formation redshift.

The virial temperature T_{vir} simply scales as $GM^{2/3}\rho^{1/3}$, where ρ is the mean cosmological gas density at the time of formation. Similarly, the initial number density of the gas at 10^4 K $n_0 \propto \rho T_{\text{vir}}$ as $n \propto 1/T$ during the cooling phase. The infall timescale, on the other hand, scales as the radius of the halo $\propto M^{1/3}\rho^{1/3}$ divided by the virial velocity $\propto T_{\text{vir}}^{1/2}$. Finally, we assume a simple power-law dependence with mass for the fraction of gas ejected in outflows, B_{out} . The most massive galaxies are expected to have negligible outflows ($B_{\text{out}} \sim 0$), while the low-mass galaxies should have higher outflow fractions that will reduce the average metal-

TABLE 2
MASS-DEPENDENT MODEL PARAMETERS

Parameter	Symbol	Scaling
Virial temperature.....	$T_{\text{vir},4}$	$\propto M_{10}^{2/3}(1+z_F)$
Initial number density at $T_4 = 1$	n_0	$\propto T_{\text{vir},4}(1+z_F)^3$
Infall timescale.....	τ_f	$\propto (1+z_F)^{-3/2}$
Outflow gas fraction.....	B_{out}	$\propto -0.3 \log M_{10}$

licity of the stellar populations, thereby blueing their colors. We use the color of faint ellipticals in local clusters to constrain B_{out} in these systems, predicting roughly $B_{\text{out}} \sim 0.6$ for $M_{10} \sim 5$. Thus, the power-law index over the mass range $5 < M_{10} < 300$ is roughly -0.3 .

Using the mass-independent parameters described in Table 1 as well as the scaling of the mass-dependent parameters shown in Table 2, we can generate a sample of galaxies starting from a luminosity function. We estimate the relative number densities of these objects using the near-infrared (NIR) H -band luminosity function of the Coma Cluster (de Propris et al. 1998), which provides a good estimate of the underlying mass function, and arrive at a final sample of galaxies studied in detail below.

Figures 3 and 4 show mass-weighted and V -band luminosity-weighted averaged ages and metallicities of the

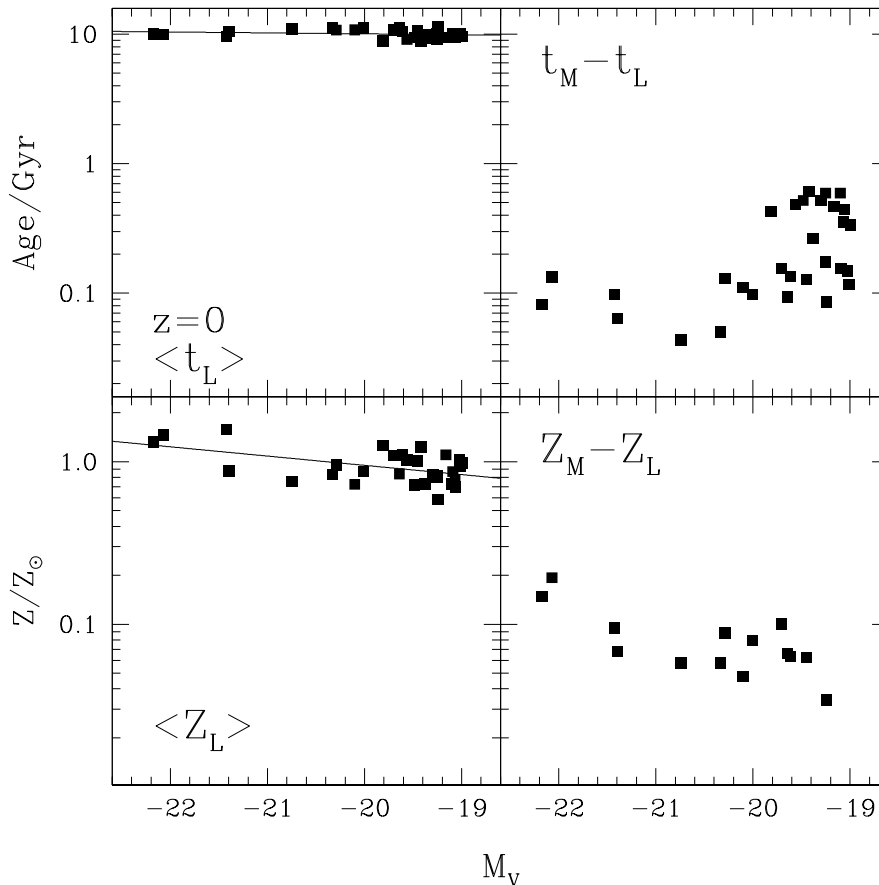


FIG. 3.—Average V -band luminosity-weighted age and metallicity (left) and its difference with a mass-weighted average (right) at zero redshift. The lines in the left-hand panels give a least-squares fit to the age-mass and metallicity-mass relations. The slopes of these linear fits are 0.02 and 0.12, respectively.

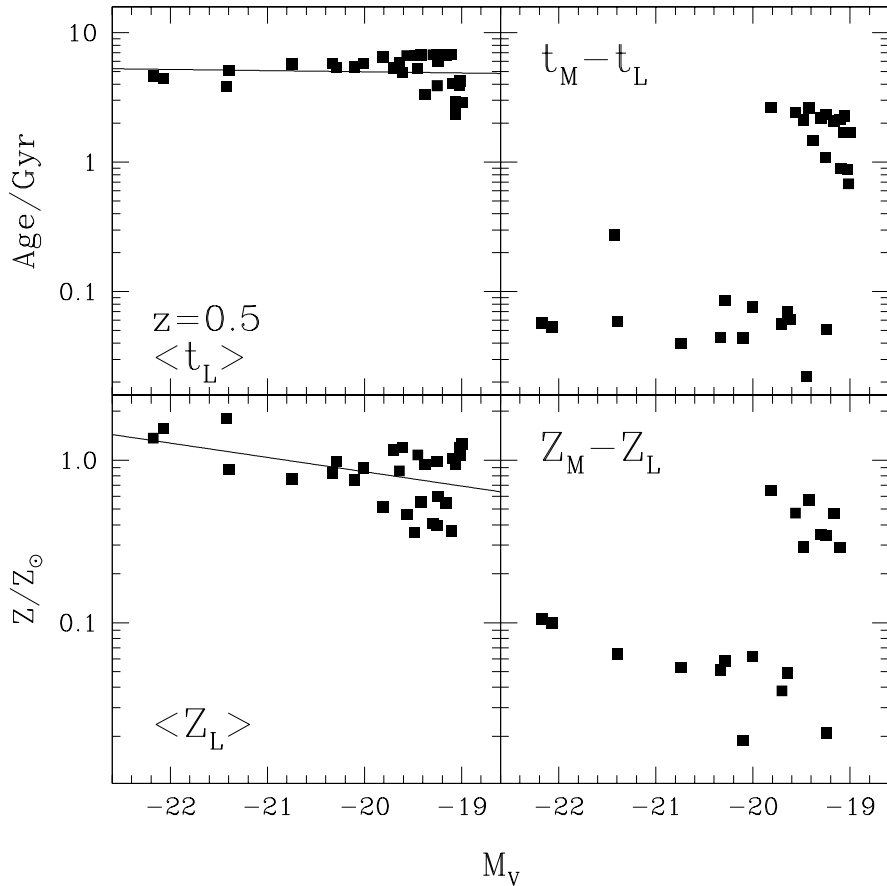


FIG. 4.—Same as Fig. 3, but for a moderate-redshift ($z = 0.5$) cluster. The slopes of the linear fits to the age-mass and metallicity-mass relations are 0.02 and 0.20, respectively.

objects, defined as

$$\langle t_M \rangle = \frac{\int_0^{t(z)} dt t \psi(t)}{\int_0^{t(z)} dt \psi(t)}, \quad (16)$$

$$\langle Z_M \rangle = \frac{\int_0^{t(z)} dt Z \psi(t)}{\int_0^{t(z)} dt \psi(t)}, \quad (17)$$

$$\langle t_L \rangle = \frac{\int_0^{t(z)} dt t \Upsilon(t)^{-1} \psi(t)}{\int_0^{t(z)} dt \Upsilon(t)^{-1} \psi(t)}, \quad (18)$$

$$\langle Z_L \rangle = \frac{\int_0^{t(z)} dt Z \Upsilon(t)^{-1} \psi(t)}{\int_0^{t(z)} dt \Upsilon(t)^{-1} \psi(t)}, \quad (19)$$

where $\Upsilon(t)$ is the V -band mass-to-light ratio as a function of stellar age and $t(z)$ is the age of the universe at the redshift at which it is observed. Comparing these results, it is clear that the ages of our model galaxies at moderate redshift are strongly dependent on which type of average is applied. While the mass-weighted values provide the most meaningful summary of the overall star formation history of the object, both photometric and spectral observations only give estimates of the luminosity-weighted age and metallicity. Thus, late episodes of star formation skew the integrated spectral energy distribution to younger ages because of the very small mass-to-light ratios of high-mass main-sequence stars.

Figure 3 shows that at zero redshift, early-type galaxies can be described by a metallicity sequence ranging from roughly $1.5 Z_\odot$ for the most massive galaxies to $0.5 Z_\odot$ for the faintest ones, in agreement with observations of ellipticals in local clusters (Kuntschner & Davies 1998; Kobayashi & Arimoto 1999). Our model gives a power-law fit between mass and metallicity of $Z \propto M^{0.15}$ at zero redshift. The slope of the age-mass relation is nearly flat at both zero and moderate ($z = 0.5$) redshift ($t \propto M^{0.02}$), although the latter presents a significantly larger scatter. While there is little difference between mass- and luminosity-weighted ages at zero redshift, Figure 4 shows significant differences at $z = 0.5$. The mass-metallicity correlation in this figure is clearly defined and has a similar power-law index: $Z \propto M^{0.20}$. However, there is an increased scatter in the luminosity-weighted ages and metallicities, especially at the faint end. This offset can be as large as a few gigayears in age, especially for galaxies with secondary bursts occurring within the previous 1 Gyr. This occurs since even small amounts of young stars can boost the luminosity mainly in the NUV, thereby reducing the luminosity-weighted age.

4. OPTICAL AND NEAR-ULTRAVIOLET COLOR-MAGNITUDE RELATIONS IN ELLIPTICALS

For a given choice of parameters, our model predicts a chemical enrichment track that determines the ages and metallicities of the stellar populations. These star formation

histories can be convolved with models of simple stellar populations to get the spectrophotometric properties of the model galaxies. To do this, we use the latest population synthesis models of G. A. Bruzual & S. Charlot (2002, in preparation) and assume a fixed baryon to total mass ratio of $\Omega_b/\Omega_m \sim \frac{1}{6}$ in order to obtain absolute luminosities.

Figure 5 gives the optical and NIR color-magnitude relation predicted for a local cluster. The model galaxies (*filled squares*) are compared with the precision photometry of Coma ellipticals observed by Bower, Lucey, & Ellis (1992; *open circles*). The solid and dashed lines are the best fits and scatter to the observations, respectively. The remarkable agreement shows that our B_{out} scaling reproduces well the expected mass-metallicity or mass-luminosity relationship (as shown in Fig. 3) that explains the color range in early-type galaxies. Notice that the $V-K$ color departs toward the blue at the faint end more than the $U-V$ color. This has to do with the higher age sensitivity of optical colors with respect to near-infrared passbands. The U and V bands will be more affected by recent episodes of star formation than K band, so that $V-K$ appears bluer than $U-V$ at the faint end at which late bursts of star formation occur.

Figure 6 shows the rest-frame 2000 Å NUV and optical color-magnitude relation predicted for two clusters at moderate redshift: A851 ($z = 0.4$; *right*), whose optical and NUV color-magnitude relation was recently analyzed by Ferreras & Silk (2000b), and Cl 0016+16 ($z = 0.55$; *left*), whose detailed optical color-magnitude relation can be found in Ellis et al. (1997). The shaded area gives the 4σ detection limit for the shallower F300W images. The solid and dashed lines show the fit and scatter to the observed data in cluster Cl 0016+16, respectively.

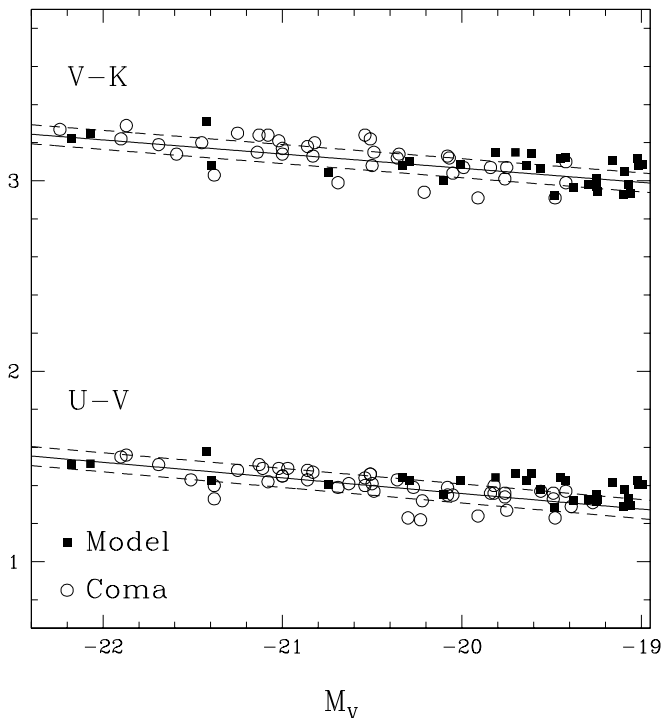


FIG. 5.—Color-magnitude relation in optical and NIR passbands for a local cluster. The filled squares are our model predictions. The open circles are Coma Cluster ellipticals observed by Bower et al. (1992). The best linear fit to the observations is given by the solid line, and the ± 0.05 mag scatter found in these galaxies is plotted as a dashed line.

These two color-magnitude relations paint two very different pictures of a similar cluster at moderate redshift. The optical colors shown in the left-hand panels do not present a large scatter. This is consistent with the observations of $z \lesssim 1$ clusters by Stanford, Eisenhardt, & Dickinson (1998), which they interpreted as an absence of star formation at redshifts below 2–3.

The NUV color-magnitude relation shown in the right-hand panels, however, points to a more involved star formation history. In this case the blue band maps a rest-frame spectral window around 2000 Å in which young main-sequence A-type stars contribute significantly, making these colors much more sensitive to recent star formation. Thus, the observed scatter with respect to the prediction for old stellar populations formed at redshifts $z \sim 5-10$ (*thick line*) is a telltale sign of recent star formation. This is particularly clear as the look-back time of this cluster allows us to safely ignore the contribution to the F300W flux from evolved, core helium burning stars, whose contribution would peak around 1500 Å. Hence, the combination of NUV and optical colors of early-type galaxies at moderate redshifts is a valuable observation for inferring the recent star formation histories of these systems. Yet detailed analyses of NUV minus optical color-magnitude relations at moderate redshift are scarce (Buson et al. 2000; Ferreras & Silk 2000b), and more work is needed in this direction.

Mass-to-light ratios are also useful stellar clocks although their observed estimates are highly model dependent. Figure 7 shows the model predictions against total mass in units of $10^{10} M_{\odot}$. Galaxies with late bursts depart from the “red envelope” since their young stars contribute significantly to the total V -band luminosity, even if they make up only a small fraction of the total stellar mass. Here the solid line is the corrected fit to the observed data from Mobasher et al. (1999; *stars*) and Pahre (1999; *open squares*), which gives $M/L_V \propto M^{0.24}$. The correction involves a slightly nonlinear power-law dependence between the stellar mass M_s and the total mass $M \propto M_s^{1.2}$ as described in Ferreras & Silk (2000c).

5. X-RAY EMISSION FROM EARLY-TYPE GALAXIES

The model presented in this paper gives the thermal state of the ISM a central role in the star formation history of elliptical galaxies. Even though our model is a rather simple one-zone system, we can use this information to predict the X-ray luminosity from the gas and its correlation with the optical luminosity, which traces the stellar component.

The X-ray luminosity of the galaxy can be approximated as arising purely from bremsstrahlung emission from free-free electron interactions. In this case

$$L_X \approx 2 \times 10^{-25} n_e N_e T_4^{1/2} \times \left(e^{-E_{\text{max}}/kT} - e^{-E_{\text{min}}/kT} \right) \text{ ergs cm s}^{-1}, \quad (20)$$

where E_{max} and E_{min} are the maximum and minimum energies of the observed X-ray band. Because of line emission, this equation is only valid at temperatures much greater than $T_4 = 1$, but this is a good assumption as the X-ray emission from cold objects is negligible. A larger source of error, in fact, is that we only include X-ray emission from the gas and not from X-ray binaries, which may contribute significantly.

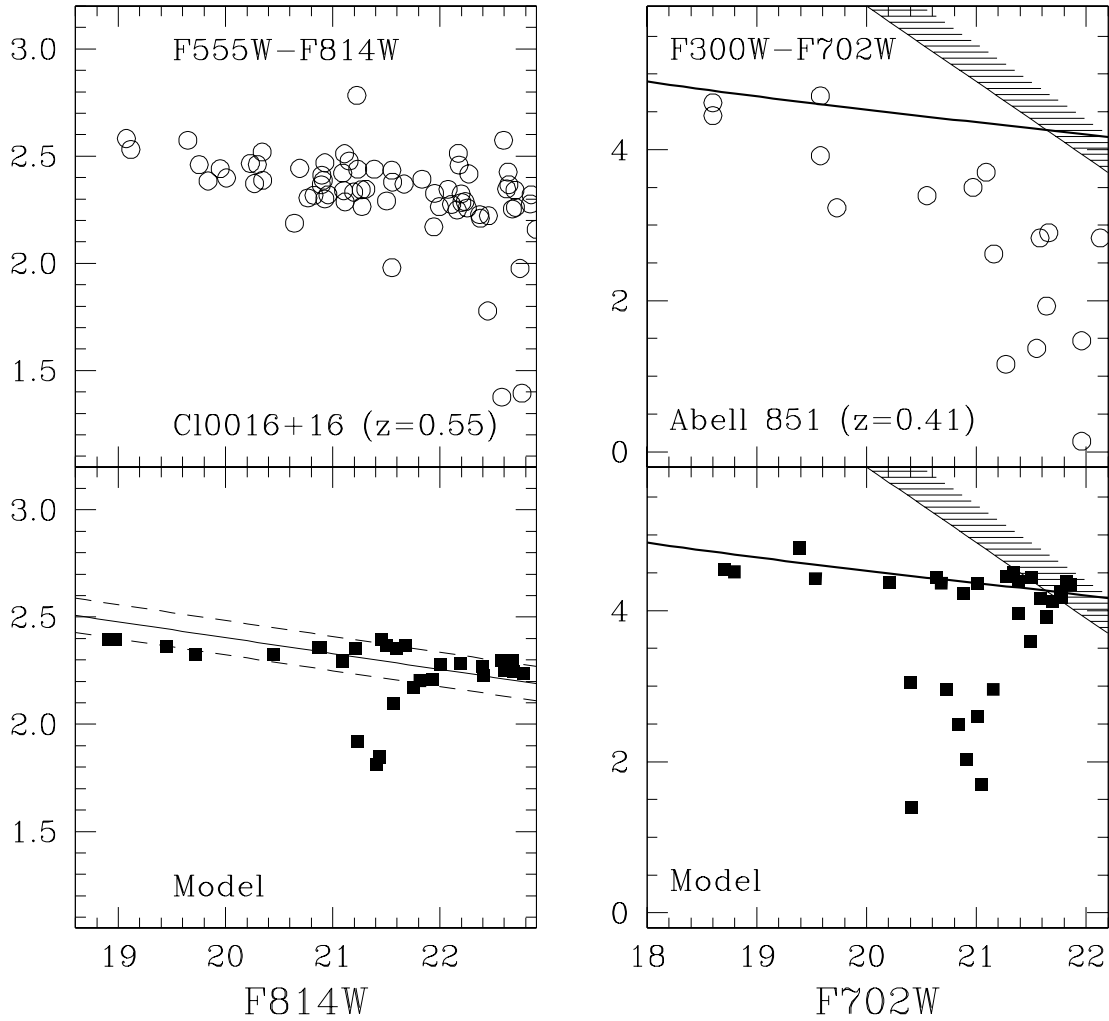


FIG. 6.—Rest-frame $U-V$ (left) and NUV minus optical (right) color-magnitude relations predicted at redshifts of $z = 0.55$ and 0.41 . The filled squares are the model predictions, whereas the open circles show the data from cluster A851 ($z = 0.41$) explored in the NUV by Ferreras & Silk (2000b) and Cl 0016+16 ($z = 0.55$) observed by the MORPHS collaboration (Ellis et al. 1997). The shaded areas in the right-hand panels give the 4σ detection limit from the shallower F300W images. The solid line in the right-hand panels gives the prediction of a single-age metallicity sequence formed at $z_F = 10$ using the color-magnitude relation of the Coma Cluster as a constraint. The solid and dashed lines in the bottom left-hand panel are the fit and scatter, respectively, to the color-magnitude relation in the elliptical galaxies of cluster Cl 0016+16.

Rewriting the number density in terms of temperature and n , using $N_e = 1.5 \times 10^{66} M_{10}$ in this cosmology, and restricting our attention to the 0.5–2.4 keV energy band, we find

$$L_X \approx (3 \times 10^{41} M_{10} n \text{ cm}^3) \mu_g T_4^{1/2} \times (e^{-530/T_4} - e^{-3400/T_4}) \text{ ergs s}^{-1}. \quad (21)$$

The filled squares in Figure 8 show the predicted L_X-L_B correlation in early-type galaxies following this equation. The open circles are taken from O’Sullivan, Forbes, & Ponman (2001), who compiled a sample of 401 early-type galaxies. The solid line gives the best fit to the observed data, excluding bright cluster and group galaxies as well as AGNs. Our model is in good agreement, showing that the trend of the L_X-L_B correlation in elliptical galaxies can be mostly explained by X-ray emission from the hot ISM. While the overall scatter in the data exceeds that in the models some-

what, this is not surprising, as the observational values are subject to additional variations due to not only the X-ray binaries as described above but perhaps also environmental effects (Mathews & Brighenti 1998).

We can also use a simple scaling argument to estimate sizes from the galaxy mass (M_{10}) and number density ($n_0 \approx nT_4$). In this case

$$R \sim 5 \text{ kpc} \left(\frac{M_{10} \mu_g}{n_0 m_{0.7}} \right)^{1/3}. \quad (22)$$

For our model galaxies the inferred sizes range from 8 to 30 kpc, which is a reasonable estimate of the core X-ray sizes of ellipticals (Mathews & Brighenti 1998). High-resolution deep X-ray images of ellipticals over a large mass range would be needed to determine the scaling of galaxy X-ray size with optical luminosity, which could quantify the contribution to the X-ray brightness from the hot interstellar gas in elliptical galaxies.

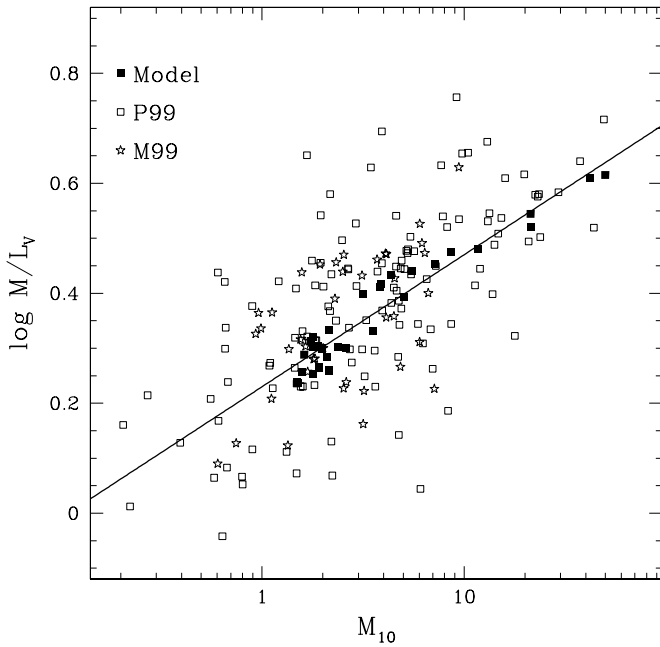


FIG. 7.—Model predictions of the V -band mass-to-light ratio vs. total mass in units of $10^{10} M_{\odot}$. The model data (*filled squares*) have been corrected for the offset between the total and the stellar mass content in elliptical galaxies (Ferreiras & Silk 2000c). The observations are from Pahre (1999; *open squares*) and Mobasher et al. (1999; *stars*).

6. TOWARD A MORE COMPLETE PICTURE OF FEEDBACK IN EARLY-TYPE GALAXIES

While our simple model of thermal feedback yields a promising explanation for many of the observed properties of early-type galaxies, it naturally raises two questions. As secondary starbursts may also arise from more complicated

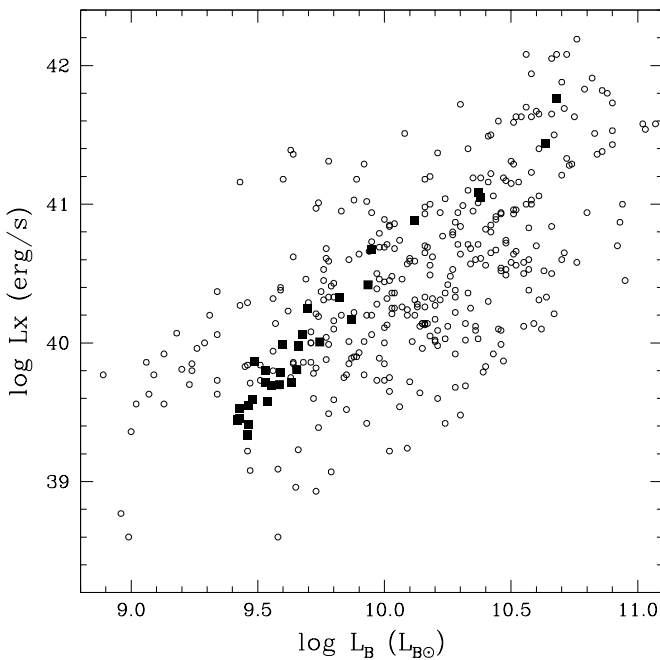


FIG. 8.—Predicted correlation between the X-ray and optical luminosities using a simple argument involving bremsstrahlung emission from the electrons in the hot gas component. The filled squares give our model predictions, whereas the open circles are from O'Sullivan et al. (2001).

gas accretion histories than the one considered here, one is left with the question of what types of observations will be most important in distinguishing between our scenario and other possibilities. Secondly, from a theoretical point of view, it is clear that intense bursts of SNe will deposit both energy and momentum over a much larger area than the ISM of the galaxy itself. This raises the question as to the uniqueness of our single-zone thermal model and whether similar feedback loops can also arise in the interplay between the galaxy and its environment. In this section we address each of these questions in turn.

6.1. Observational Implications

The elliptical star formation histories described in this paper are much more complicated than those of more usual models that assume a short epoch of star formation resulting in stellar populations with well-defined ages and metallicities. Although our predictions for massive galaxies are quite similar to such models, our lower mass systems experience secondary episodes of star formation that affect their luminosities, particularly at moderate redshifts. This is true independent of the possibility of other sources of late star formation from environmental effects.

Our conclusion clearly calls for more detailed analyses of elliptical galaxies at moderate and high redshift. It also gives an additional mechanism for “hiding” high-redshift ellipticals from view. In fact, this possibility is reminiscent of the blue-nucleated field early-type galaxies observed by Menanteau, Abraham, & Ellis (2001) in the Hubble Deep Field, which may be examples of the late bursts predicted by our model. Similarly, the poststarburst E+A galaxies found in clusters are suggestive of our results.

It is also interesting to note that the observed correlation between abundance ratio enhancements and galaxy mass or luminosity (Kuntschner & Davies 1998; Trager et al. 2000) is indicative of extended star formation in low-mass galaxies, which allows the by-products from Type Ia SNe to be locked into subsequent generations of stars. Galaxies with central velocity dispersions around 50 km s^{-1} , for example, tend to have $[\text{Mg}/\text{Fe}]$ ratios close to solar, while values around $[\text{Mg}/\text{Fe}] \sim 0.3$ are observed in massive ($\sigma_0 \sim 400 \text{ km s}^{-1}$) galaxies. Again, this hints at late bursts of star formation.

While the short duration of our secondary bursts makes their direct detection a complicated endeavor, observations of NUV colors may provide a tractable approach to studying feedback. As young main-sequence A-type stars have strong Balmer absorption lines in the NUV spectral window around 2000 \AA , observations that map this rest-frame wavelength can be used to trace recent star formation. Thus, while low numbers of cluster galaxies with strong emission lines are seen at moderate redshift (Dressler et al. 1999), up to 20% of such galaxies feature poststarburst NUV spectra (Poggianti et al. 1999). The large scatter at the faint end of the NUV minus optical color-magnitude relation of A851 (Ferreiras & Silk 2000b) is a further indication of the sensitivity of this approach. As the thermal feedback mechanism presented in this paper is independent of the environment, comparisons of these colors in the field, groups, and cluster populations should provide a direct method of separating the contribution of thermal feedback to star formation in spheroids from other processes.

6.2. Alternative Models of Feedback

The model of feedback in elliptical galaxies we have examined in this paper focuses on ISM heating, modulating star formation by changing the condition of the gas within the galaxy itself. However, the presence of a large number of SNe following a burst of star formation is likely to also deposit significant amounts of energy and momentum into the surrounding intergalactic medium. In our thermal model, infall onto the galaxy was fixed simply by the dynamical timescale of a virialized cloud as a function of mass and redshift. While this is a reasonable approximation at early times, the rate of infall from the intergalactic medium after the onset of star formation may be slowed as a result of collisions with SN ejecta. This raises the question as to whether multiple starbursts can also arise in models that focus on the interplay between the galaxy and its environment.

To study the features of such models, we can replace our simple two-component model with a three-component model in which we track stars, the gas contained within the galaxy, and a second gas reservoir that represents the surrounding medium, which is condensing onto the galaxy. In order to isolate the features of such an approach from the thermal effects discussed above, we do not attempt to track the temperature of the gas but rather consider a generic set of equations describing a broad class of models in which infall is modulated by feedback. In this case we find

$$\begin{aligned}\dot{\mu}_g &= \mu_r/\tau - \epsilon_{\text{mom}}E - C_{\text{eff}}\mu_g + (1-f)(1-B_{\text{out}})E, \\ \dot{\mu}_r &= -\mu_r/\tau + \epsilon_{\text{mom}}E + f(1-B_{\text{out}})E, \\ \dot{\mu}_s &= C_{\text{eff}}\mu_g,\end{aligned}\quad (23)$$

where ϵ_{mom} is a parameter of order $(10^{51} \text{ ergs}/M_{\odot})^{1/2}/v_{\text{vir}} \approx 10/v_{100}$ that parameterizes the suppression of infall by SNe, f is the fraction of ejected material that is recycled into the infalling reservoir, and the infall is now parameterized as an exponential with a scale time τ in order to simplify the analytical arguments below.

With these equations in hand we now approximate the behavior of this system using a “post”-instantaneous recycling approximation in which we model $E(t)$ considering the timescale (τ_2) corresponding to the lifetime of stars that play a role in stellar feedback. In this approximation we write the ejected fraction as

$$E(t) \sim C_{\text{eff}}f_{\text{SN}}[\mu_g(t) - \dot{\mu}_g(t)\tau_2], \quad (24)$$

where f_{SN} is the gas fraction returned by SNe. Note that a good estimate of τ_2 is ~ 0.02 Gyr (roughly the lifetime of a massive star that undergoes core collapse, i.e., $M \sim 10 M_{\odot}$), but we are also free to take $\tau_2 = 0$, recovering the more commonly studied instantaneous recycling approximation.

Rewriting these equations in terms of the infall timescale and defining $s \equiv t/\tau_1$, $\mathcal{C} = C_{\text{eff}}\tau_1$, and $x \equiv \tau_2/\tau_1$, we find

$$(1 - \mathcal{C}L) \frac{d^2\mu_g}{ds^2} + (1 + \mathcal{C}M) \frac{d\mu_g}{ds} + \mathcal{C}N\mu_g = 0, \quad (25)$$

where $L \equiv f_{\text{SN}}\epsilon'x$, $M \equiv 1 + f_{\text{SN}}\epsilon' + (1 - B_{\text{out}})f_{\text{SN}}x$, $N \equiv 1 - (1 - B_{\text{out}})f_{\text{SN}}$, and $\epsilon' \equiv \epsilon_{\text{mom}} - (1 - f)(1 - B_{\text{out}})$. Note that for any reasonable choice of parameters $\epsilon' > 0$ as $\epsilon_{\text{mom}} \approx 10/v_{100}$ is much greater than $(1 - f)(1 - B_{\text{out}})$. Thus, L , M , and N are greater than 0 in all physical models.

Equation (25) is the equation for a harmonic oscillator, $\ddot{y} + \gamma\dot{y} + \omega_0^2y = 0$. If we define $\Omega \equiv (\omega_0^2 - \gamma^2/4)^{1/2}$, then the criterion for oscillation is $\Omega > 0$, which can be rewritten as

$$4\mathcal{C}N(1 - \mathcal{C}L) - (1 + \mathcal{C}M)^2 > 0. \quad (26)$$

In the limit in which \mathcal{C} is very small or large this inequality is never satisfied, and likewise at its local maximum $\mathcal{C} = (2N - M)/(M^2 + 4NL)$. Thus, we see that for a very general class of models in which infall is modulated by star formation, no oscillations are present in the post-instantaneous recycling approximation.

As an additional check, we have solved equation (23) numerically over a broad range of parameters, blanketing the relevant physical values. These results confirm the analytical arguments above, showing that oscillations never take place in models that modulate infall as long as $\epsilon' \equiv \epsilon_{\text{mom}} - (1 - f)(1 - B_{\text{out}})$ is positive.

7. CONCLUSIONS

While stellar feedback in galaxy formation has been the subject of intense theoretical investigation, these studies have had little impact on the direct interpretation of the observed properties of elliptical galaxies. However, there are several observational clues that point to its importance. Ferreras & Silk (2000c), for example, found that the color-magnitude relation of early-type cluster galaxies can be easily understood in the context of a variable ejection efficiency of SN material, which scales inversely with galaxy mass. Similarly, the large scatter in the faint end of the NUV minus optical color-magnitude relation in early-type cluster galaxies hints at episodic star formation in these objects, a natural consequence of stellar feedback (Ferreras & Silk 2000b).

Motivated by these observational and theoretical pointers, we have explored in this work a simple model of thermal feedback in elliptical galaxies. Our model consists of only gas and stars in a single zone and is a natural extension of previous investigations (Tinsley 1980; Ferreras & Silk 2000c, 2001), which includes the thermal state of the ISM. We account for heating by SN feedback and line emission cooling, as well as their impact on the temperature and density of the ISM using a minimum of parameters, and relate these quantities to the overall star formation rate using a Schmidt law and a temperature-dependent efficiency. This model is applicable in the case in which the time for SNe to percolate through the ISM is sufficiently long that spatial variations between regions are relatively unimportant. While this is the case for the choice of parameters adopted in this paper, more detailed modeling is necessary to study the interplay between thermalization and substructure conclusively.

Our model leads to two important and independent results. First, the interplay between infall and variable SN ejection efficiency provides a natural explanation of the optical and NIR color-magnitude relations in elliptical galaxies both locally and at moderate redshift ($z \lesssim 1$). Our model generates a mass-metallicity relation $Z \propto M^{0.15-0.2}$, which accounts for the observed color range over 3 mag in luminosity. Furthermore, the rapid cooling times for temperatures close to 10^4 K result in short bursts of star formation, generating stellar populations that are very similar to the simple ones commonly used to describe ellipticals. This

implies no change in the slope or the scatter of the optical and NIR color-magnitude relation out to redshifts $z \lesssim 1$ as observed by many authors (e.g., Stanford et al. 1998; van Dokkum et al. 1998, 2000).

Second, we find that secondary peaks of late star formation are ubiquitous in smaller systems in which the fraction of the SN ejecta that escapes from the ISM, B_{out} , is significant. In these cases the gas is heated to temperatures $\propto (1 - B_{\text{out}})$, leading to secondary bursts of star formation with a delay that scales as $\propto (1 - B_{\text{out}})^3$ as a result of the T^3 scaling of the cooling times of high-temperature gas. As such bursts occur within a Hubble time only in the smaller galaxies in which B_{out} is relatively large, this leads to a natural explanation of the large scatter in the NUV-optical relation as observed in clusters at moderate redshifts. This can also account for the observed population of poststarburst E+A galaxies that display a spheroidal morphology (Ferreiras & Silk 2000a). While the current claim for these poststarburst systems is the quenching of star formation while falling through the hot intracluster medium (Poggianti et al. 1999), our model shows that late starbursts may arise in elliptical galaxies without resorting to environmental mechanisms. In fact, we have found that no such oscillations arise in a broad class of theoretical models that study the interplay between SNe and the further accretion of gas.

Given that the duration of these peaks of star formation is rather short (~ 100 Myr), the most promising observational approach is to examine the NUV properties of spheroidal galaxies. A comprehensive study of the rest-frame NUV minus optical color-magnitude relation in ellipticals may be able to quantify both the number of galaxies that undergo late bursts and the mass fraction in young stars. Furthermore, as the thermal mechanism studied in this paper is independent of environment, comparisons of such colors between field, group, and cluster populations can help to differentiate between this feedback and other processes. As the contribution in the NUV from evolved core helium burning stars becomes significant with age, studies of galaxies at redshifts $z \gtrsim 0.3$ may provide the cleanest samples for such comparisons.

At $z \gtrsim 1$, late bursts can be significant even in high-mass galaxies, as shown in Figure 1. This may result in the failure of any search for high-redshift ellipticals that is based on simple passively evolving models and does not invoke complicated scenarios of assembly (e.g., Zepf 1997). Our model also underscores the bias intrinsic to observing luminosity-weighted quantities. While the mass- and luminosity-weighted ages of higher mass ellipticals are quite similar,

even the relatively small bursts of late star formation that arise in smaller objects cause large changes in their observed V -band luminosity-weighted ages. This effect is even more severe in the NUV, highlighting the importance accounting for the overall star formation history when interpreting observed stellar ages.

One of the remarkable results of our model is the presence of an ISM that has been heated by SNe to temperatures around 1 keV or higher. This hot gas exists at very low densities, with only a fraction leaving the galaxy, much in the same way as the hot gas of the solar corona is kept gravitating around the Sun. A full three-dimensional simulation would be needed in order to explore the real conditions under which this “fountain effect” can occur.

Finally, our prediction of a hot corona of SN-heated gas has natural implications for the X-ray properties of elliptical galaxies. By approximating the overall X-ray luminosity of each object as due to bremsstrahlung emission from gas at the single temperature and density given by our model, we derive an L_X - L_B correlation that is in good agreement with observed values. Nevertheless, our simple one-zone model does not account for environmental effects and ignores what is likely to be a significant contribution from unresolved X-ray binaries, resulting in a scatter that is smaller than observed.

Galaxy formation is one of the richest and most complex processes in all of astrophysics, forcing observers and theorists to approach it from completely different viewpoints. Although both theoretical and observational progress has been clear and systematic, the rift between theory and observation in the field remains one of the most difficult to bridge. In this work, we have attempted to draw the key theoretical issue of feedback into the direct interpretation of the observational properties of early-type galaxies. While our approach has been explorational, the widespread agreement of our simple model with diverse observations suggests that thermal feedback processes are likely to be essential to fully understanding the optical, ultraviolet, and X-ray properties of early-type galaxies.

I. F. is supported by a grant from the European Community under contract HPMF-CT-1999-00109. E. S. is supported by a National Science Foundation MPS-DRF postdoctoral fellowship. I. F. gratefully acknowledges the hospitality of the Astronomy Department at the University of California, Berkeley. We thank Ewan O’Sullivan for making available the X-ray data of early-type galaxies used in this paper.

REFERENCES

- Arimoto, N., & Yoshii, Y. 1987, *A&A*, 173, 23
 Balbi, A., et al. 2000, *ApJ*, 545, L1
 Baugh, C. M., Cole, S., Frenk, C. S., & Lacey, C. G. 1998, *ApJ*, 498, 504
 Bower, R. G., Lucey, J. R., & Ellis, R. S. 1992, *MNRAS*, 254, 601
 Buson, L. M., Bertola, F., Cappellari, M., Chiosi, C., Dressler, A., & Oemler, A. 2000, *ApJ*, 531, 684
 de Propris, R., Eisenhardt, P. R., Stanford, S. A., & Dickinson, M. 1998, *ApJ*, 503, L45
 Dressler, A., Smail, I., Poggianti, B. M., Butcher, H., Couch, W. J., Ellis, R. S., & Oemler, A., Jr. 1999, *ApJS*, 122, 51
 Eisenstein, D., & Hu, W. 1999, *ApJ*, 511, 5
 Eke, V. R., Cole, S., & Frenk, C. S. 1996, *MNRAS*, 282, 263
 Ellis, R. S., et al. 1997, *ApJ*, 483, 582
 Ferreras, I., & Silk, J. 2000a, *ApJ*, 532, 193
 ———. 2000b, *ApJ*, 541, L37
 ———. 2000c, *MNRAS*, 316, 786
 ———. 2001, *ApJ*, 557, 165
 Gerritsen, J. P. E. 1997, Ph.D. thesis, Kapteyn Astron. Inst.
 Greggio, L., & Renzini, A. 1983, *A&A*, 118, 217
 Hultman, J., & Pharasyn, A. 1999, *A&A*, 347, 769
 Katz, N. 1992, *ApJ*, 391, 502
 Kauffmann, G., & Charlot, S. 1998, *MNRAS*, 294, 705
 Kauffmann, G., Colberg, J. M., Diaferio, A., & White, S. D. M. 1999, *MNRAS*, 303, 188
 Kennicutt, R. C., Jr. 1998, *ApJ*, 498, 541
 Kobayashi, C., & Arimoto, N. 1999, *ApJ*, 527, 573
 Kroupa, P. 2001, *MNRAS*, 322, 231
 Kuntschner, H., & Davies, R. L. 1998, *MNRAS*, 295, L29
 Larson, R. B. 1999, in *Star Formation 1999*, ed. T. Nakamoto (Nobeyama: Nobeyama Radio Observatory), 336
 Mac Low, M. M., & Ferrara, A. 1999, *ApJ*, 513, 142
 Marigo, P., Bressan, A., & Chiosi, C. 1996, *A&A*, 313, 545
 Martel, H., & Shapiro, P. R. 2001, *Rev. Mexicana Astron. Astrofis. Ser. Conf.*, 10, 101
 Mathews, W. G., & Brighenti, F. 1998, *ApJ*, 493, L9
 Matteucci, F., & Recchi, S. 2001, *ApJ*, 558, 351
 Matteucci, F., & Tornambè, A. 1987, *A&A*, 185, 51
 McKee, C. F., & Ostriker, J. P. 1977, *ApJ*, 218, 148

- Menanteau, F., Abraham, R. G., & Ellis, R. S. 2001, MNRAS, 322, 1
- Mihos, J. C., & Hernquist, L. 1994, ApJ, 437, 611
- Mobasher, B., Guzmán, R., Aragón-Salamanca, A., & Zepf, S. 1999, MNRAS, 304, 225
- Nakamura, F., & Umemura, M. 2001, ApJ, 548, 19
- Navarro, J., & Benz, W. 1991, ApJ, 380, 320
- Netterfield, C. B., et al. 2002, ApJ, 571, 604
- Nomoto, K., Iwamoto, K., & Kishimoto, N. 1997, Science, 276, 1378
- O'Sullivan, E., Forbes, D. A., & Ponman, T. J. 2001, MNRAS, 328, 461
- Pahre, M. A. 1999, ApJS, 124, 127
- Poggianti, B. M., Smail, I., Dressler, A., Couch, W. J., Barger, A. J., Butcher, H., Ellis, R. S., & Oemler, A., Jr. 1999, ApJ, 518, 576
- Pryke, C., et al. 2002, ApJ, 568, 46
- Renzini, A. 1999, in Chemical Evolution from Zero to High Redshift, ed. J. R. Walsh & M. R. Rosa (Berlin: Springer), 185
- Renzini, A., & Voli, A. 1981, A&A, 94, 175
- Salpeter, E. E. 1955, ApJ, 121, 161
- Scalo, J. 1998, in ASP Conf. Ser. 142, The IGM Revisited: A Case For Variations, ed. G. Gilmore & D. Howell (San Francisco: ASP), 201
- Scannapieco, E., & Broadhurst, T. 2001, ApJ, 549, 28
- Scannapieco, E., Thacker, R. J., & Davis, M. 2001, ApJ, 557, 605
- Somerville, R. S., & Primack, J. R. 1999, MNRAS, 310, 1087
- Springel, V. 2000, MNRAS, 312, 859
- Stanford, S. A., Eisenhardt, P. R., & Dickinson, M. 1998, ApJ, 492, 461
- Sutherland, R. S., & Dopita, M. A. 1993, ApJS, 88, 253
- Tantalo, R., Chiosi, C., Bressan, A., Marigo, P., & Portinari, L. 1998, A&A, 335, 823
- Thacker, R. J., & Couchman, H. M. P. 2001, ApJ, 555, L17
- Thielemann, F. K., Nomoto, K., & Hashimoto, M.-A. 1996, ApJ, 460, 408
- Thielemann, F. K., Nomoto, K., & Yokoi, K. 1986, A&A, 158, 17
- Thomas, D., Greggio, L., & Bender R. 1999, MNRAS, 302, 537
- Tinsley, B. M. 1980, Fundam. Cosmic Phys., 5, 287
- Trager, S. C., Faber, S. M., Worthey, G., & González, J. J. 2000, AJ, 119, 1645
- Vader, J. P. 1986, ApJ, 305, 669
- van den Hoek, L. B., & Groenewegen, M. A. T. 1997, A&AS, 123, 305
- van Dokkum, P. G., Franx, M., Fabricant, D., Illingworth, G. D., & Kelson, D. D. 2000, ApJ, 541, 95
- van Dokkum, P. G., Franx, M., Kelson, D. D., Illingworth, G. D., Fisher, D., & Fabricant, D. 1998, ApJ, 500, 714
- White, S. D. M. 1994, in Les Houches Summer School, Cosmology and Large-Scale Structure, ed. R. Schaeffer, J. Silk, M. Spiro, & J. Zinn-Justin (Amsterdam: North-Holland), 1
- Woosley, S., & Weaver, T. 1995, ApJS, 101, 181
- Worthey, G., Dorman, B., & Jones, L. A. 1996, AJ, 112, 948
- Yepes, G., Kates, R., Khokhlor, a., & Klypin, A. 1997, MNRAS, 284, 235
- Zepf, S. E. 1997, Nature, 390, 377